Generation of envelope and hole solitons in an experimental transmission line

P. Marquie,* J. M. Bilbault, and M. Remoissenet
Physique Non Linéaire: Laboratoire Ondes et Structures Cohérentes, Faculté des Sciences, 6 Boulevard Gabriel, 21000 Dijon, France
(Received 23 July 1993)

We study the generation of nonlinear modulated waves in an experimental electrical transmission line. Our theoretical analysis, based on the nonlinear Schrödinger equation, predicts three frequency regions with different behavior concerning the modulational instability of a plane wave. These predictions are confirmed by our experiments which show that, between two modulationally stable frequency bands where hole solitons can be generated, there is a third band, where spontaneous or induced modulational instability occurs and where envelope solitons exist. The experimental shapes of both hole and envelope solitons are well fitted by the theoretical waveforms, which take into account the damping due to the components.

PACS number(s): 03.40.Kf, 84.40.Mk

I. INTRODUCTION

In nonlinear dispersive media, the propagation of modulated waves, such as envelope (bright) solitons or hole (dark) solitons, has been the subject of considerable interest for many years. In nonlinear optics [1–6], the recent important progress about fiber loss allows the improvement of practical results concerning the distortionless signal transmission in ultrahigh-speed communications.

On the other hand, discrete electrical transmission lines are very convenient tools to study the wave propagation in one-dimension (1D) nonlinear dispersive media [7]. In particular, they provide a useful way to check how the nonlinear excitations behave *inside* the nonlinear medium and to model the exotic properties of new systems [8]. Several authors have shown that the electrical transmission lines allow the formation of modulational instability [9–10] and the eventual formation of envelope solitons [11–13]; the existence of hole solitons was also studied [12–14]. Nevertheless, although these experiments are interesting, they are rather qualitative and there is a need to investigate systematically the remarkable properties of nonlinear modulated waves.

It is the main purpose of this paper to present a careful and quantitative experimental analysis concerning modulational instability and the generation of either envelope or hole solitons on the same transmission line, depending on an appropriate choice of the carrier wave frequency. The outline of the paper is as follows. In Sec. II we present the characteristics of our nonlinear electrical network. We show that the system of nonlinear equations governing the physics of the network can be reduced to a nonlinear Schrödinger (NLS) equation. In Sec. III we describe the experiments and present the results concerning the formation of hole solitons; the modulational instability of an initial plane wave and the related generation of envelope solitons are studied. The influence of dissipation is then investigated in Sec. IV. In the final section, we give some concluding remarks.

II. THEORY

A. Modulated waves and the nonlinear Schrödinger model

We consider a nonlinear network with N cells, as illustrated in Fig. 1. Each cell contains a linear inductance L_1 in series and a linear inductance L_2 in parallel with a nonlinear capacitance C. This capacitance consists of a reverse-biased diode. It is biased by a constant voltage V_0 and depends on the voltage V_n at cell n such as

$$C(V_0+V_n)=\frac{dQ_n}{dV_n}=C_0[1-2\alpha V_n+3\beta V_n^2+\cdots], \tag{2.1}$$

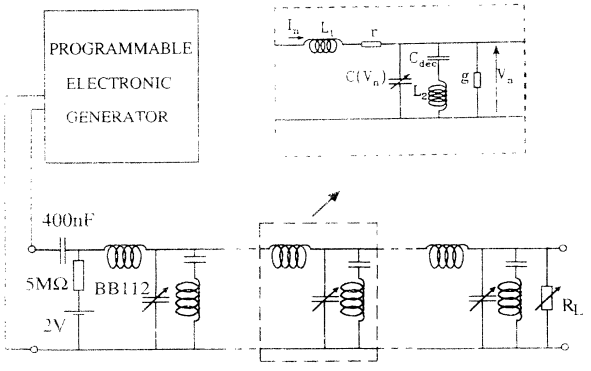

FIG. 1. Schematic representation of the experimental arrangement. The network is composed of 45 cells identical with that presented above. Each diode BB112 with nonlinear capacitance is biased by 2 V through a resistance of 5 MΩ. Linear decoupling capacitances C_{dec} are used to block the dc biased current but have no effect at the considered frequency range.

*Electronic address:
MARQUIE@SATIE.U-BOURGOGNE.FR

where the coefficients α and β are positive. In (2.1), we keep nonlinear coefficients up to the second order for the following reasons. First, the polynomial approximation of the *C-V* curve and corresponding fit are justified if the voltage amplitude is small enough: $V_n < 2$ V. Second, in this voltage range, to reduce the equation of motion [see (2.2) hereafter] to an NLS equation (2.9), it is sufficient to take into account these two terms, only, to balance the first-order dispersion term.

The inductances L_1 and L_2 have, respectively, a resistance r and a conductance g. In a previous article [15] we have shown that the dissipation due to r was negligible with respect to that due to g; therefore we do not take it into account in our calculations. From Kirchhoff's laws, we derive the system of nonlinear discrete equations

$$\frac{d^2V_n}{dt^2}+\omega_0^2V_n+u_0^2gL_1\frac{dV_n}{dt}+u_0^2(2V_n-V_{n+1}-V_{n-1}) =\alpha\frac{d^2V_n^2}{dt^2}-\beta\frac{d^2V_n^3}{dt^2}\ , \quad n=1,2,\ldots,N \tag{2.2}$$

with $u_0^2=1/L_1C_0$ and $\omega_0^2=1/L_2C_0$.

In the linear ($V_n \ll 1$) and nondissipative ($g\simeq 0$) approximation, from (2.2) we get the linear dispersion relation of a typical bandpass filter

$$\omega^2=\omega_0^2+4u_0^2\sin^2\frac{k}{2}\ . \tag{2.3}$$

The linear dispersion curve corresponding to (2.3) is shown in Fig. 2, where $f_0=\omega_0/2\pi$ is the lower cutoff frequency introduced by the parallel inductance L_2, and

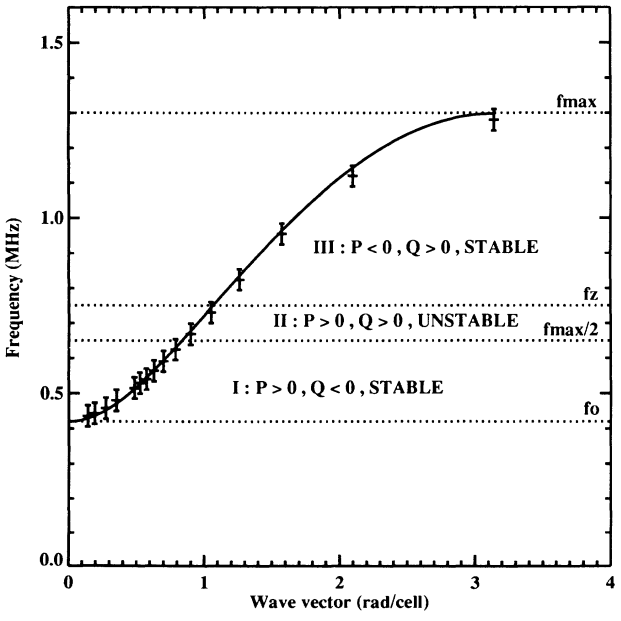

FIG. 2. Theoretical and experimental linear dispersion curves. The allowed band $[f_0, f_{\max}]$ is divided into three regions concerning the stability of the system, relative to the sign of PQ.

$$f_{\max}=\frac{\omega_{\max}}{2\pi}=\frac{1}{2\pi}\left[\frac{1}{L_2C_0}+\frac{4}{L_1C_0}\right]^{1/2} \tag{2.4}$$

is the cutoff frequency introduced by the lattice effects. The corresponding linear group velocity and dispersion coefficient are

$$v_g=\frac{\partial\omega}{\partial k}=\frac{u_0^2\sin k}{\omega},\quad P=\frac{\partial^2\omega}{\partial k^2}=\frac{u_0^2\cos k-v_g^2}{2\omega}\ . \tag{2.5}$$

It is important to note that there exists a frequency $f=f_z$ making the dispersion coefficient become zero (see Fig. 2).

We focus on modulated waves with a slowly varying envelope in time and space with regard to a given carrier wave with angular frequency $\omega=\omega_p=2\pi f_p$ and wave number $k=k_p$. Then, in order to use the reductive perturbation method [16], we introduce the slow envelope variables $X=\epsilon(n-v_gt)$ and $\tau=\epsilon^2t$, where ϵ is a small parameter and n is the cell number. Moreover, the solution of (2.2) is assumed to have the following general form:

$$V_n(t)=\epsilon\mathcal{V}_1(X,\tau)e^{j\theta} +\epsilon^2[\mathcal{V}_0(X,\tau)+\mathcal{V}_2(X,\tau)e^{2j\theta}]+\text{c.c.}, \tag{2.6}$$

with $\theta=(k_pn-\omega_pt)$. The dc and second-harmonic terms, respectively, $\mathcal{V}_0(X,\tau)$ and $\mathcal{V}_2(X,\tau)$, are added to the fundamental one, $\mathcal{V}_1(X,\tau)$, in order to take into account the asymmetry of the charge-voltage relation.

Now, from the observation of the dispersion curve (Fig. 2) let us make *the following simplifications, which are of crucial importance in the present investigation.*

(i) First, the dc term $\mathcal{V}_0(X,\tau)$ will vanish due to the existence of the low-frequency forbidden band.

(ii) Second, when examining the S-shaped dispersion curve, one remarks that twice the frequency does not correspond to twice the wave vector [17]. This implies that the $\mathcal{V}_2(X,\tau)e^{2j\theta}$ term does not represent the real second harmonic. Owing to nonlinearity, this signal exists and does not propagate because it does not satisfy the dispersion relation (2.3). Thus we must replace Eq. (2.6) by

$$V_n(t)=\epsilon\mathcal{V}_1(X,\tau)e^{j\theta_1} +\epsilon^2[\mathcal{V}_2(X,\tau)e^{2j\theta_1}+\mathcal{V}_2'(X,\tau)e^{j\theta_2}]+\text{c.c.}, \tag{2.7}$$

with $\theta_1=\theta=(k_pn-\omega_pt)$ and $\theta_2=(Kn-2\omega_pt)$, where K is the wave number that satisfies the dispersion relation for $\omega=2\omega_p$.

(iii) Third, when $f_p > f_{\max}/2$, all the harmonics have their frequency lying above the cutoff frequency $f_{\max}$. In this case, (2.7) reduces to

$$V_n(t)=\epsilon\mathcal{V}_1(X,\tau)e^{j\theta_1}+\text{c.c.} \tag{2.8}$$

In summary, when using the reductive perturbation method in the semidiscrete limit, we have to consider (2.7) for $f_0 < f_p < f_{\max}/2$, and (2.8) for $f_{\max}/2 < f_p < f_{\max}$. Focusing on the first case, we substitute (2.7) in (2.2). Then, assuming $g=\epsilon^2g_1$, to order ϵ^3 we get the nonlinear Schrödinger equation governing the

slow envelope evolution

$$j\frac{\partial \mathcal{V}_1}{\partial \tau}+P\frac{\partial^2 \mathcal{V}_1}{\partial X^2}+j\Gamma \mathcal{V}_1+Q|\mathcal{V}_1|^2\mathcal{V}_1=0 , \tag{2.9}$$

where

$$P=\frac{u_0^2\cos k_p-v_g^2}{2\omega_p},$$

$$Q=Q_1=\omega_p\left|\frac{3\beta}{2}-\frac{4\alpha^2\left[\omega_0^2+4u_0^2\sin^2\frac{k_p}{2}\right]}{3\omega_0^2+16u_0^2\sin^4\frac{k_p}{2}}\right| , \tag{2.10}$$

$$\Gamma=\frac{g_1}{2C_0}$$

represent dispersion, nonlinearity, and dissipation, respectively.

In the second case, we assume a solution of the form (2.8) and get another NLS equation similar to (2.9), except for the nonlinear coefficient, which is

$$Q=Q_2=\tfrac{3}{2}\beta\omega_p . \tag{2.11}$$

Importantly, when Q_1 is negative, Q_2 is positive and only depends on the nonlinear coefficient β, i.e., the electrical network behaves as if the capacitance-voltage relation (2.1) would be quadratic only. Regions of positive and negative dispersion, and regions of positive and negative nonlinearity are reported in Fig. 2.

B. Hole and envelope soliton solutions

We now turn our attention to the soliton solutions of the NLS equation. It is well known that a plane-wave solution of (2.9) is modulationally stable if $PQ<0$. On the contrary, for $PQ>0$, the system is modulationally unstable in the Benjamin-Feir sense [18] if the wave vector K and the angular frequency Ω of the perturbation satisfy the following conditions:

$$\begin{aligned} &0<K<K_{cr}=A_0\left|\frac{2Q}{P}\right|^{1/2} ,\\ &0<\Omega<\Omega_{cr}=2\pi F_{cr}=v_gK_{cr} . \end{aligned} \tag{2.12}$$

As time goes on, the modulation increases and the continuous wave breaks into a periodic pulse or envelope soliton train. The wave vector $K_{\max}$ and the angular frequency $\Omega_{\max}$ of the modulation corresponding to the maximum of instability are given by

$$K_{\max}=A_0\left|\frac{Q}{P}\right|^{1/2} , \quad \Omega_{\max}=2\pi F_{\max}=v_gK_{\max} . \tag{2.13}$$

Next, when $PQ<0$, as it is in regions I and III, we have a hole soliton solution [19] given by

$$V(n,t)=2A_0\left[1-\alpha^2\operatorname{sech}^2\left\{\left|\left|\frac{Q}{2P}\right|\right|^{1/2}\alpha A_0(n-v_gt)\right\}\right]^{1/2}\cos[k_pn-\omega_pt-\theta(n,t)] , \tag{2.14}$$

where $2A_0$ is the real amplitude at $|n|\to\infty$, α is a parameter related to the depth of modulation, and $\theta(n,t)$ is the phase function given by

$$\theta(n,t)=\left|\left|\frac{Q}{2P}\right|\right|^{1/2}A_0\sqrt{1-\alpha^2}(n-v_gt)+\arctan\left\{\frac{\alpha}{\sqrt{1-\alpha^2}}\tanh\left|\left|\frac{Q}{2P}\right|\right|^{1/2}\alpha A_0(n-v_gt)\right\}+\frac{Q}{2}(3-\alpha^2)A_0^2t . \tag{2.15}$$

The spatial width of the soliton defined at half height is

$$L_h=\frac{2}{\alpha A_0}\left|\left|\frac{2P}{Q}\right|\right|^{1/2}\operatorname{sech}^{-1}\left|\frac{1}{2\alpha}\sqrt{\alpha^2-2\sqrt{1-\alpha^2}+2}\right| , \tag{2.16}$$

and to first order, this soliton travels at group velocity v_g.

On the other hand, for $PQ>0$ (region II), Eq. (2.9) admits envelope or bright soliton solutions [19] of the form

$$V(n,t)=2A_0\operatorname{sech}\left|\left|\frac{Q}{2P}\right|^{1/2}A_0(n-v_gt)\right|\cos(k_pn-\omega_pt) , \tag{2.17}$$

which to first order travel at group velocity v_g. As for the hole soliton, one defines the spatial width at half height

$$L_e=2\left|\frac{2P}{QA_0^2}\right|^{1/2}\operatorname{sech}^{-1}(\tfrac{1}{2}) . \tag{2.18}$$

In summary, we have three different regions concerning the modulational instability of a plane wave and the possible soliton solutions:

$$f_p \in \begin{cases} \left[f_0, \dfrac{f_{\max}}{2}\right], & PQ_1 < 0 \rightarrow \text{stable} \rightarrow \text{hole solitons, region I} \\ \left[\dfrac{f_{\max}}{2}, f_z\right], & PQ_2 > 0 \rightarrow \text{unstable} \rightarrow \text{envelope solitons, region II} \\ [f_z, f_{\max}], & PQ_2 < 0 \rightarrow \text{stable} \rightarrow \text{hole solitons, region III} \end{cases} \quad (2.19)$$

The nonlinear behavior of the electrical network is also summarized in Fig. 2.

III. EXPERIMENTAL STUDY

Our experiments are carried out on a nonlinear electrical network (Fig. 1) with $N=45$ identical cells. The nonlinear capacitance consists of a varicap diode (BB112), biased by a constant voltage $V_0=2$ V. Under these conditions one has $C_0=320\pm10$ pF, $\alpha=0.21$ V^{-1}, and $\beta=0.0197$ V^{-2}. The linear inductances are $L_1=220\pm5$ μH and $L_2=470\pm10$ μH, whereas the total Ohmic losses are, respectively: $r=5$ Ω and $g=1.3\times10^{-5}$ Ω^{-1}. The line is matched by a variable resistor. The waves are created by using a programmable arbitrary function generator [20]. The waveforms can be observed and stored by using a numerical oscilloscope (Lecroy 9450) with fast-Fourier-transform processing. The oscilloscope probes have high impedance (10 MΩ) and small capacitance (15 pF) in order to avoid parasitic reflections.

In the linear or very-small-amplitude approximation, the dispersion curve which is that of a bandpass filter is measured as follows. At the input of the line we apply a sinusoidal voltage of low amplitude $V_{\text{input}}=100$ mV supplied by a generator with internal resistance 50 Ω. Results are plotted in Fig. 2: the agreement with the theoretical dispersion curve given by relation (2.3) is quite good. The measured lower cutoff frequency is $f_0=435\pm10$ kHz and the higher cutoff frequency is $f_{\max}=1280\pm30$ kHz.

A. Scanning of the stable and unstable regions

In order to check our theoretical predictions (2.19), we investigate the stability of a plane wave of larger amplitude, say $A_0=0.56$ V, over the whole frequency range: $f_0<f_p<f_{\max}$. Our theory predicts instability for $f_{\max}/2<f_p<f_z$. Experimentally, for $f_0<f_p<620$ kHz$\simeq f_{\max}/2$, no instability is detected. On the contrary, an instability develops for 620 kHz$<f_p<720$ kHz$\simeq f_z$, leading to a self-modulation of the wave as represented for cell number $n=9$ on the oscillograms shown in Figs. 3(a) and 3(b). This instability occurs spontaneously; it is induced by the electrical noise that is present along the electrical network. It is important here to make sure that the observed instability is not due to both propagating and counterpropagating waves. In this case, the modulational instability conditions would be quite different [21]. Then, the load resistance has to be carefully adjusted in order to minimize the reflected waves. From the Fourier spectrum [Fig. 3(c)], the measured frequency of the envelope modulation is $F=70$ kHz, a value that is quite smaller than the theoretical one $F_{\max}=178$ kHz provided by relation (2.13). Nevertheless, it lies in the instability domain $0<F<F_{\text{cr}}=252$ kHz predicted by (2.12).

On the other hand, we can also consider the instability that can be induced by a coherent and weak external modulation [22]. Namely, we launch a sinusoidal wave with frequency $f_p=670$ kHz slightly amplitude modulated (19%) as shown in Fig. 4(a). For an appropriate value of the modulation frequency, instability develops leading to the increase of the modulation. Namely, at cell number $n=12$, and for $A_0=0.19$ V, the modulation increases and becomes maximum (34%) when the envelope frequency F is about 60 kHz, as represented in Fig. 4(b). The frequency F, measured from the Fourier spectrum shown in Fig. 4(c), agrees very well with the theoretical value $F_{\max}=61$ kHz calculated from (2.13). Consequently, our experimental results are in good agreement with our theoretical predictions (2.19) in spite of the approximations we have made. Finally, for 720 kHz$<f_p<f_{\max}$,

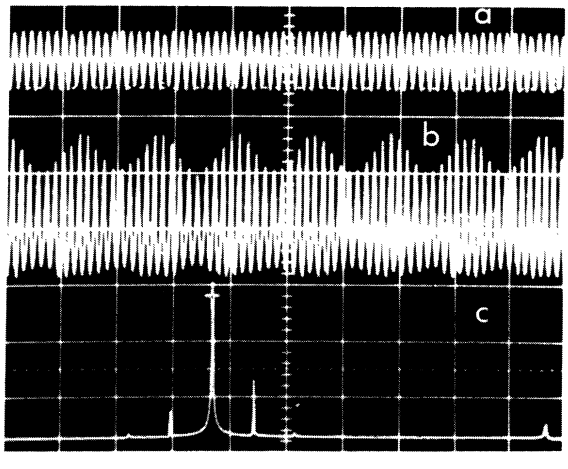

FIG. 3. Spontaneous modulational instability: the continuous plane wave provided by the generator breaks into a periodic pulse train under the action of electronic noise. (a) Initial plane wave at $f_p=670$ kHz, with 4-V amplitude peak to peak. Abscissa: 10 μs/div. Ordinate: 4 V/div. (b) Signal at cell number $n=9$. Abscissa: 10 μs/div. Ordinate: 2 V/div. (c) Fast-Fourier transform (FFT) of the signal at cell number $n=9$. The carrier frequency (central peak) is 670 kHz and its amplitude is $2A_0=1.13$ V. The side bands due to modulation are ±70 kHz away. Ordinate: 450 mV/div.

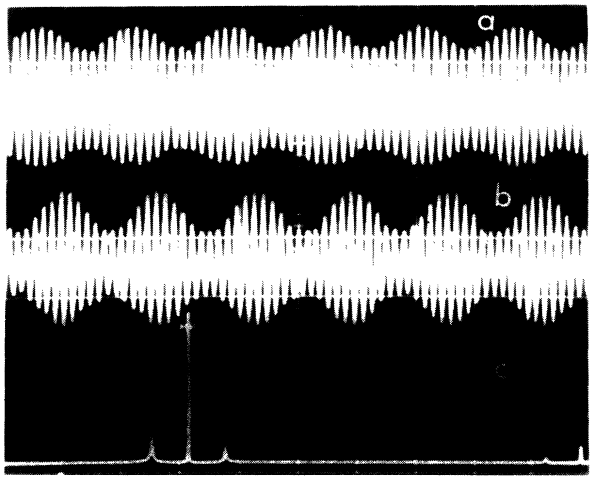

FIG. 4. Induced modulational instability. (a) Initial wave at the input of the line with a 19% rate of modulation. The carrier wave frequency is $f_p = 670$ kHz while the modulation frequency is $F = 60$ kHz. Abscissa: 10 μs/div. Ordinate: 500 mV/div. (b) Modulated wave at cell number $n = 12$. Here, the rate of modulation is 34%. Abscissa: 10 μs/div. Ordinate: 500 mV/div. (c) FFT of the signal at cell number $n = 12$. The carrier frequency (central peak) is 670 kHz and its amplitude is $2A_0 = 0.38$ V. The side bands due to modulation are ± 60 kHz away. Ordinate: 165 mV/div.

FIG. 5. Oscillogram of a hole soliton. (a) Initial condition supplied by a generator. Abscissa: 10 μs/div. Ordinate: 1 V/div. (b) Waveform at cell number $n = 41$. Abscissa: 10 μs/div. Ordinate: 200 mV/div.

by contrast to (2.19) which predicts stability, some frequency windows are detected that present instabilities. This may be due to discreteness effects which are partially taken into account in our semidiscrete approach yielding the NLS equation. This complex problem is not examined here and is left for further investigations. We now analyze carefully the behavior of the network in regions I and II.

B. Region I: Hole solitons

In this region, from (2.19), we expect hole solitons. In fact, in spite of dissipative effects, a hole soliton can be generated in the network by launching a hole-shaped initial signal. In Figs. 5(a) and 5(b) we present the oscillograms corresponding to the hole-shaped wave supplied by the generator with a carrier wave frequency $f_p = 600$ kHz and the hole soliton at the 41th cell. Theoretically, for $f_p = 600$ kHz, one finds $P = 6.15 \times 10^5$ rad s^{-1}, $Q = -2.8 \times 10^5$ V^{-2} rad s^{-1}, and $v_g = 2.4$ cell μs^{-1}. Then, for $2A_0 = 310$ mV at cell number $n = 41$, the width at half height calculated by relation (2.16) is $L_h = 22$ cells. These theoretical predictions are verified by our experimental results; indeed, one measures a propagation velocity $v_{\text{exp}} = v_g = 2.4 \pm 0.1$ cell μs^{-1}, and the experimental width at half height is $L_{h,\text{expt}} = 24 \pm 3$ cells.

In Fig. 6 the shape of the experimental hole soliton shown in Fig. 5(b) is compared with the theoretical waveform (2.14) for $2A_0 = 310$ mV and $\alpha = 0.934$. The fitting is good, except for the difference between the theoretical curve and the negative part of the experimental envelope. In fact, this discrepancy is due to the existence of a second harmonic that renders the envelope asymmetric and was not taken into account in the theoretical calculations (2.14).

By launching an initial wave packet with its carrier wave frequency f_p in region I, we have checked that an envelope soliton cannot form along the network. Namely, the wave packet spreads out very quickly. This result is consistent with the fact that theory predicts the existence of hole solitons only.

C. Region II: Envelope solitons

Theory predicts that envelope solitons can exist in this region. In fact, they can be created by launching an ini-

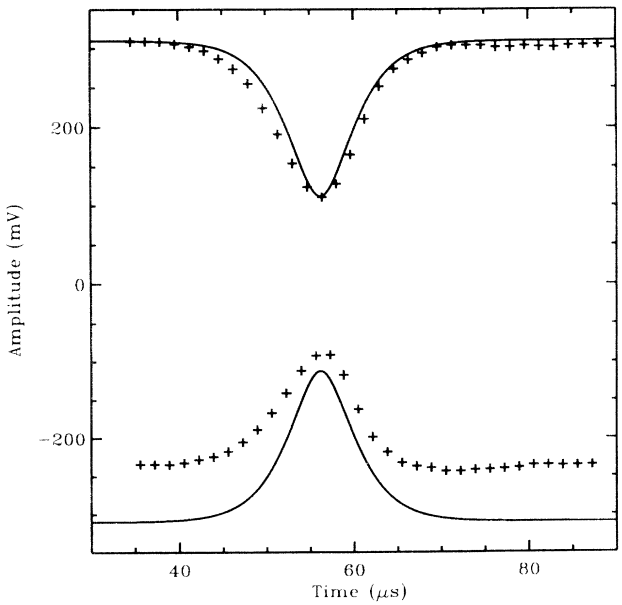

FIG. 6. Theoretical and experimental waveforms of the hole soliton presented in Fig. 5(b).

tial wave packet which becomes an envelope soliton. The oscillograms showing the initial wave packet with $f_p=670$ kHz and the envelope soliton at cell number $n=41$ are presented, respectively, in Figs. 7(a) and 7(b). The measured propagation velocity and temporal width at half height are, respectively, $v_{\text{expt}}=2.5\pm0.1$ cell μs^{-1} and $T=8.2\pm0.5$ μs. So, one gets the experimental spatial width at half height $L_{e,\text{expt}}=v_{\text{expt}}T=21\pm3$ cells. The velocity of the soliton corresponds to the theoretical group velocity (2.5) calculated for $f_p=670$ kHz that is $v_g=2,5$ cell μs^{-1}. Again, the experimental width at half height agrees with the theoretical one: $L_e=24$ cells, calculated from relation (2.18) with $P=2.10^5$ rad s^{-1}, $Q=1.25\times10^5$ V^{-2} rad s^{-1}, and the amplitude $2A_0=400$ mV for $n=41$. The experimental envelope shown in Fig. 7(b) is well fitted by the theoretical expression (2.17) as is presented in Fig. 8, if one eliminates from the data the influence of the linear tail that follows the soliton.

On the other hand, if we try to launch an initial wave that is hole shaped, in order to generate a hole soliton, it is strongly perturbed. Specifically, after a few sections, the modulation depth decreases and the hole spreads out. Again, in this case our result is consistent with theory, which predicts the existence of envelope solitons only.

Now, let us make the following remarks. First, for hole solitons, good agreement between theoretical predictions and experiments is also obtained in the lower part of region III. However, when the carrier-wave frequency lies in one of the strong dispersion regions, i.e., the lower part of region I and the higher part of region III, the generation of hole solitons becomes impossible. In fact, it suggests to use a new approach to fully take into account the discreteness effects.

Second, in our experiments, we verify that envelope solitons have a constant phase. On the contrary, the phase function (2.15) of the hole soliton is supposed to present a jump at the soliton center [23]. In fact, we notice experimentally a nonconstant phase versus time or space, but it does not present the predicted shape. The shortness of the line compared to the soliton size could be the reason why the soliton properties are modified.

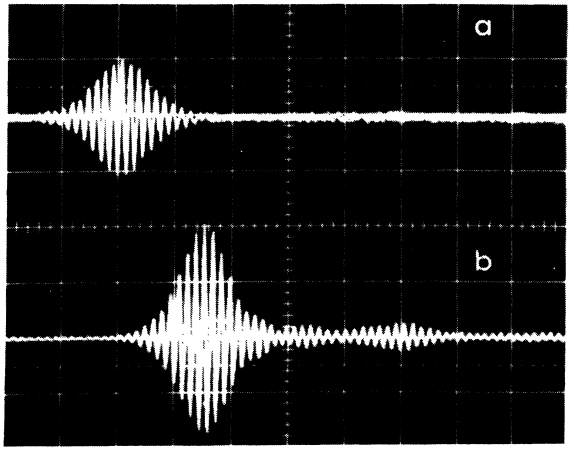

FIG. 7. Oscillograms of an envelope soliton. (a) Initial condition created by the generator. Abscissa: 10 μs/div. Ordinate: 1 V/div. (b) Pulse at cell number $n=41$. Abscissa: 10 μs/div. Ordinate: 200 mV/div.

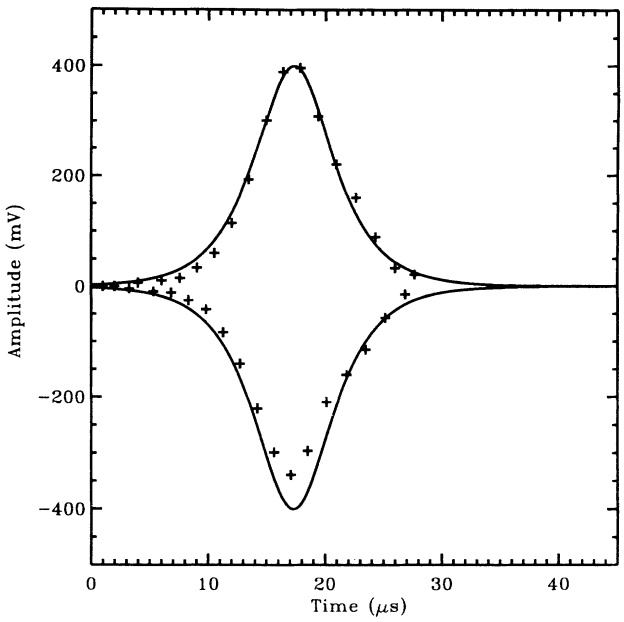

FIG. 8. Theoretical and experimental waveforms of the envelope soliton presented in Fig. 7(b).

IV. INFLUENCE OF DISSIPATION

Until now, we have ignored the influence of dissipation for the study of modulational instability as well as for the generation of hole or envelope solitons. Nevertheless, experimental results agree relatively well with the theoretical predictions of Sec. II, namely, for the existence of three frequency bands as predicted by (2.19). However, dissipation exists because one can measure a decay of soliton amplitudes.

Concerning envelope solitons, theory predicts that, if in NLS Eq. (2.9) dissipation is taken into account (see, e.g., Hasegawa [19]), we have to replace A_0 by $A_0e^{-2\Gamma n/v_g}$ in (2.17) and (2.18). Consequently, the amplitude of the envelope soliton decreases exponentially twice as for a linear wave, while its spatial width increases as $e^{2\Gamma n/v_g}$.

To check this prediction, we consider an envelope soliton with a carrier-wave frequency $f_p=670$ kHz and we carefully study how its amplitude decays along the line, as illustrated in Fig. 9(a). Note the dispersion of the experimental points due to standing waves that originate from weak inhomogeneities along the line. A least-squares fit (continuous line) gives a damping constant $\gamma=0.019$ cell^{-1}. Then, let us consider the propagation of a plane wave with a small amplitude and a frequency $f_p=670$ kHz [Fig. (9b)]. This linear wave decays exponentially versus the cell number with a damping constant $\gamma'=0.010$ cell^{-1}. This value agrees with the theoretical linear decay in the laboratory frame $\Gamma/v_g=g/2C_0v_g=0.008$ cell^{-1}, obtained from the linear-

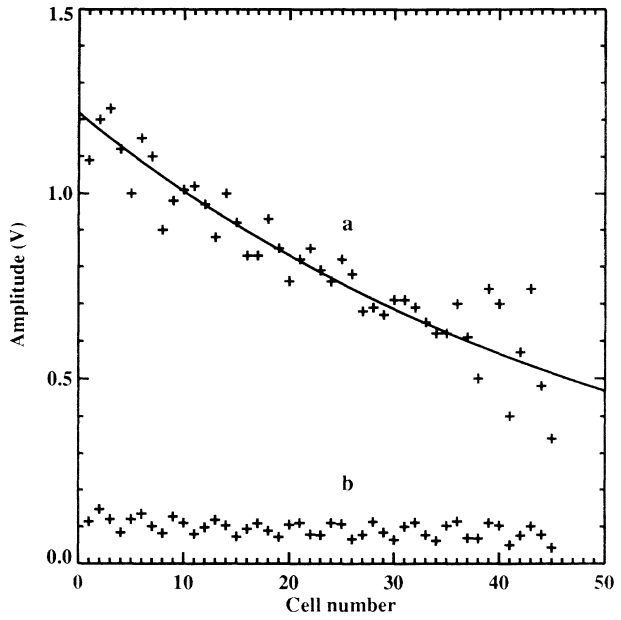

FIG. 9. Dissipation influence along the line for an envelope soliton (a) and a linear plane wave (b). The carrier wave frequency is $f_p = 670$ kHz for both.

ized version of (2.9).

Thus, our results confirm the theoretical prediction [19]; that is, the damping constant of the envelope soliton is twice more important in the nonlinear case with respect to the linear one, i.e., $\gamma' = 2\gamma = 2\Gamma/v_g$. On the other hand, no significant spreading of the width at half height is detected. This can be due to the shortness of the network as compared with the size of the solitons.

Focusing finally on hole solitons, we know from the literature [24–28] that the spreading due to dissipation is the same as for the linear case; that is, the spatial width increases as $e^{\Gamma n/v_g}$. Nevertheless, in this case, we have been unable to detect the increase of the spatial width, probably due to the size of the soliton with respect to the length of the lattice. In summary, dissipation acts on the amplitude of the soliton but not on its profile, and it would be interesting now to built a longer and less dissipative line, allowing us to study how the soliton profile evolves under dissipation.

V. CONCLUSION

In this paper, we have examined the possibility of generating either envelope or hole solitons in an electrical transmission line. Theoretically, we have shown that the system of nonlinear equations governing the physics of the electrical network can be reduced to an NLS equation. From this analysis three different regions can be predicted: between two modulationally stable regions where hole solitons can be generated there exists a third region where spontaneous or induced modulational instability can occur and where envelope solitons can be generated.

Next, we have experimentally found the three regions predicted by the theory. In regions I and III, that is, for 435 kHz $< f_p <$ 620 kHz and 720 kHz $< f_p <$ 1280 kHz, respectively, no instability is detected and it is possible to generate hole solitons. The experimental shape of these solitons is well fitted by the theoretical waveform, in spite of the approximations we have made. On the contrary, in region II, that is, for 620 kHz $< f_p <$ 720 kHz, spontaneous or induced modulational instability occurs, and the characteristic wave number and frequency measured for the induced modulational instability agree very well with those predicted by the theory. Furthermore, envelope solitons can be generated in this region, and again, the fitting of the experimental envelope by the theoretical waveform is good.

The dissipation effects have been discussed. We have found a good agreement between theoretical predictions and experiments concerning the influence of the dissipation on the envelope soliton amplitude, that is, the damping constant is twice more important in the nonlinear case with respect to the linear one. On the other hand, it has not been possible to measure the influence of dissipation on the profile of the soliton, the length of the network being too short with respect to the size of the soliton. Our results suggest that the losses must be reduced in order to improve the propagation of solitons. This is currently under investigation.

Finally, our results confirm that our electrical transmission line is a very interesting model for studying the specific properties of 1D nonlinear systems. Both types of nonlinear localized modulated waves, envelope and hole solitons, can be generated in the same system by means of an appropriate choice of the carrier wave frequency.

ACKNOWLEDGMENT

The authors are grateful to B. Michaux for his invaluable technical assistance.

[1] A. Hasegawa and F. Tappert, Appl. Phys. Lett. **23**, 142 (1973).
[2] A. Hasegawa and F. Tappert, Appl. Phys. Lett. **23**, 171 (1973).
[3] L. F. Mollenauer, R. H. Stolen, and G. P. Gordon, Phys. Rev. Lett. **45**, 1095 (1980).
[4] D. Krökel, N. J. Halas, G. Giuliani, and D. Grischkowsky, Phys. Rev. Lett. **60**, 29 (1988).
[5] A. M. Weiner, J. P. Heritage, R. J. Hawkins, R. N. Thurston, E. M. Kirschner, D. E. Leaird, and W. J. Tomlinson, Phys. Rev. Lett. **61**, 2445 (1988).
[6] L. F. Mollenauer, M. J. Neubelt, S. G. Evangelides, J. P. Gordon, J. R. Simpson, and L. G. Cohen, Opt. Lett. **15**, 1203 (1990).
[7] A. C. Scott, *Active and Nonlinear Wave Propagation in Electronics* (Wiley, Interscience, New York, 1970).
[8] K. E. Lonngren, in *Soliton in Action,* edited by K. E. Lonngren and A. C. Scott (Academic, New York, 1978).
[9] T. Yagi and A. Noguchi, Electron Commun. Jpn. **59A**, 1 (1976).

[10] K. Fukushima, J. Phys. Soc. Jpn. **52**, 376 (1983).
[11] K. Fukushima, M. Wadati, and Y. Narahara, J. Phys. Soc. Jpn. **49**, 1593 (1980).
[12] K. I. Volyak, V. F. Marchenko, and A. M. Strel'Tsov, Sov. Phys. Lebedev Inst. Rep. (USA) **4**, 53 (1987).
[13] K. I. Volyak, V. F. Marchenko, and A. M. Strel'Tsov, Radiophys. Quantum Electron. **31**, 954 (1988).
[14] K. Muroya, N. Saitoh, and S. Watanabe, J. Phys. Soc. Jpn. **51**, 1024 (1982).
[15] P. Marquie and J. M. Bilbault, Phys. Lett. A **174**, 250 (1993).
[16] T. Taniuti and N. Yajima, J. Math. Phys. (N.Y.) **10**, 1369 (1969).
[17] A. Hirose and K. E. Lonngren, *Introduction to Wave Phenomena* (Wiley Interscience, New York, 1985), p. 329.
[18] T. B. Benjamin and J. E. Feir, J. Fluid Mech. **27**, 417 (1967).
[19] A. Hasegawa, in *Optical Solitons in Fibers, Second Enlarged Edition* (Springer-Verlag, Berlin, 1989).
[20] B. Michaux (unpublished).
[21] D. Barday and M. Remoissenet, Phys. Rev. B **43**, 7297 (1991).
[22] A. Hasegawa, Opt. Lett. **9**, 288 (1984).
[23] W. J. Tomlinson, R. J. Hawkins, A. M. Weiner, J. P. Heritage, and R. N. Thurston, J. Opt. Soc. Am. B **6**, 329 (1989).
[24] W. Zhao and E. Bourkoff, Opt. Lett. **14**, 703 (1989).
[25] S. A. Gredeskul, Y. S. Kivshar, and M. V. Yanovskaya, Phys. Rev. B **41**, 3994 (1990).
[26] J. A. Giannini and R. I. Joseph, IEEE J. Quantum Electron. **26**, 2109 (1990).
[27] M. Lisak, D. Anderson, and B. A. Malomed, Opt. Lett. **16**, 1936 (1991).
[28] Y. S. Kivshar, IEEE J. Quantum Electron. **29**, 250 (1993).

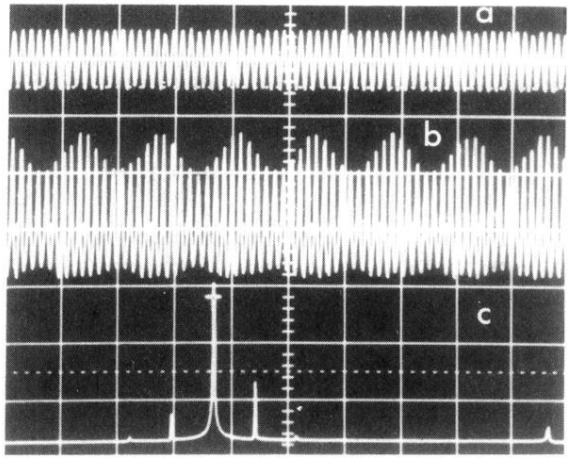

FIG. 3. Spontaneous modulational instability: the continuous plane wave provided by the generator breaks into a periodic pulse train under the action of electronic noise. (a) Initial plane wave at $f_p = 670$ kHz, with 4-V amplitude peak to peak. Abscissa: 10 μs/div. Ordinate: 4 V/div. (b) Signal at cell number $n = 9$. Abscissa: 10 μs/div. Ordinate: 2 V/div. (c) Fast-Fourier transform (FFT) of the signal at cell number $n = 9$. The carrier frequency (central peak) is 670 kHz and its amplitude is $2A_0 = 1.13$ V. The side bands due to modulation are ± 70 kHz away. Ordinate: 450 mV/div.

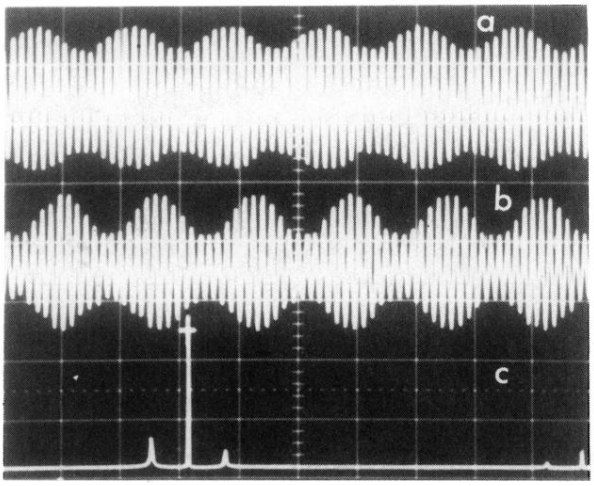

FIG. 4. Induced modulational instability. (a) Initial wave at the input of the line with a 19% rate of modulation. The carrier wave frequency is $f_p = 670$ kHz while the modulation frequency is $F = 60$ kHz. Abscissa: 10 μs/div. Ordinate: 500 mV/div. (b) Modulated wave at cell number $n = 12$. Here, the rate of modulation is 34%. Abscissa: 10 μs/div. Ordinate: 500 mV/div. (c) FFT of the signal at cell number $n = 12$. The carrier frequency (central peak) is 670 kHz and its amplitude is $2A_0 = 0.38$ V. The side bands due to modulation are ± 60 kHz away. Ordinate: 165 mV/div.

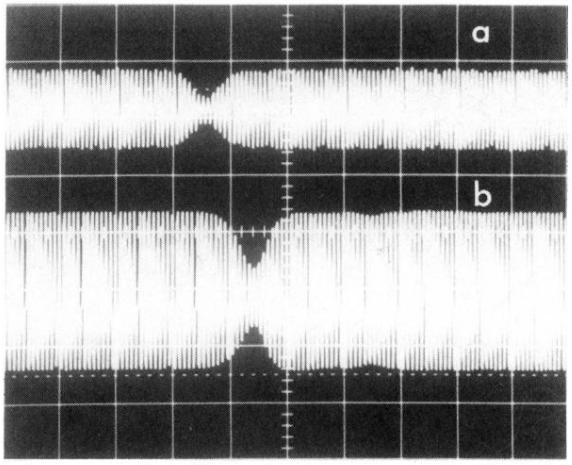

FIG. 5. Oscillogram of a hole soliton. (a) Initial condition supplied by a generator. Abscissa: 10 μs/div. Ordinate: 1 V/div. (b) Waveform at cell number $n=41$. Abscissa: 10 μs/div. Ordinate: 200 mV/div.

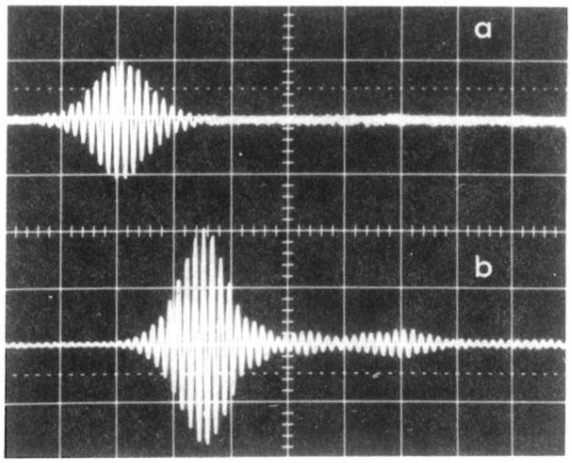

FIG. 7. Oscillograms of an envelope soliton. (a) Initial condition created by the generator. Abscissa: 10 μs/div. Ordinate: 1 V/div. (b) Pulse at cell number $n = 41$. Abscissa: 10 μs/div. Ordinate: 200 mV/div.